AIAA SciTech Forum
6-10 January 2025, Orlando, FL
AIAA SCITECH 2025 Forum

10.2514/6.2025-0073

Check for updates

Liutex-based Sub-grid Model for Large Eddy Simulation of Turbulent Flow

Emran Hossen[1] , Yifei Yu[2], Chaoqun Liu[3], Jiawei Chen[4]

The University of Texas at Arlington, Arlington, Tx, 76019, USA

Zhining Liu[5]

HyperComp, Inc, Westlake Village, CA, 91361, USA

Yonghua Yan[6]

Jackson State University, Jackson, MS, 39217, USA

Vishwa Shah[7,] Oscar Alvarez[8]

The University of Texas at Arlington, Arlington, Tx, 76019, USA

Downloaded by Emran Hossen on March 25, 2025 | http://arc.aiaa.org | DOI: 10.2514/6.2025-0073

Large eddy simulation (LES) is a popular approach for turbulent flow. The key issue is to find a proper sub-grid model to represent the filtered sub-grid scales (SGS). Currently, most people still use eddy viscosity to construct the SGS model. Smagorinsky sub-grid model is a popular and classical model for LES, which in general overestimates the eddy viscosity near the wall surface and creates a large discrepancy with direct numerical simulation (DNS) and experiment results. Liutex is a newly proposed vortex definition and identification method that can correctly represent flow rotation or vortex. A Liutex-based SGS model is applied in this paper to do the LES for the backward step flow, channel flow and flat plate boundary transition. Computational results show that Liutex-based SGS model outperforms the classic Smagorinsky model. Eddy is vortex and therefore can be measured by Liutex. Liutex can represent eddy viscosity more properly and accurately. The Liutex-based sub-grid model gives zero eddy viscosity in the laminar sublayer, which is consistent with physics while Smagorinsky model cannot as they partially use non-rotating shear to measure the eddy viscosity.

I. Introduction

In turbulent flow, vortices or eddies are the main building blocks of the turbulent flows which consist of numerous numbers of vortices with different sizes and strengths. To understand turbulence mechanisms and structures, it is therefore important to define and identify vortices. However, people did not find a proper definition of vortex until the concept of Liutex, a third generation vortex identification method, [1] proposed in 2018. Vortex identification methods are classified into three generations by Liu et al [2]. Vorticity and vorticity-related methods are the first generation (G1) methods. Eigenvalue-based methods such as Q criterion etc. are the second generation (G2) methods.

[1] Ph.D. Student, Department of Mathematics.
[2]Assistant Professor of Research, Department of Mathematics.
[3] Professor, Department of Mathematics.
[4] Assistant Professor of Research, Department of Mathematics.
[5] Member Technical Staff, HyperComp, Inc.
[6] Assistant Professor, Mathematics & Statistical Science.
[7] Ph.D. Student, Department of Mathematics
[8] Ph.D. Student, Department of Mathematics

Copyright © 2025 by the American Institute of Aeronautics and Astronautics, Inc. All rights reserved.

Liutex is the third generation (G3) method. G1 and G2 methods are contaminated by shear and/or stretching while Liutex represents the rigid rotation [3,4]. Liutex is an eigenvector-based vortex identification concept whose direction is parallel to the local rotation axis and whose magnitude is twice angular speed. Essentially, vorticity can be decomposed into rotating and non-rotating parts[5], with the rotational part being a Liutex vector. Liutex is defined[6] mathematically as follows:

$$\boldsymbol{R} = R\boldsymbol{r} = \left\{ \langle \boldsymbol{\omega}, \boldsymbol{r} \rangle - \sqrt{\langle \boldsymbol{\omega}, \boldsymbol{r} \rangle^2 - 4\lambda_{ci}^2} \right\} \boldsymbol{r} \tag{1}$$

where $\boldsymbol{\omega}$ is the vorticity vector and $\boldsymbol{r}$ is the eigenvector of the velocity gradient matrix, λ_{ci} is the imaginary part of the complex eigenvalues of the velocity gradient matrix and $\langle \cdot, \cdot \rangle$ represents inner product.

The Navier-Stokes equations, which characterize fluid flow, were developed by Claude-Louis Navier [7] and George Gabriel Stokes [8]; however, solving them analytically is difficult because of their nonlinear terms. Despite the mysterious characteristics of turbulence, developments such as direct numerical simulation (DNS) have enhanced people's comprehension, which is in general expensive, and the turbulent flow can be numerically modeled through several other computational methods, including large eddy simulation (LES) and Reynolds-averaged Navier-Stokes (RANS). DNS is a computational fluid dynamics (CFD) approach for solving the Navier-Stokes equations numerically without any turbulence model. This approach requires resolving all temporal and spatial scales of turbulence. In contrast, RANS computes time-average equations of motion for fluid flow. DNS provides more accurate results but has a high demand for computation resources while RANS is the opposite. LES is a compromise of DNS and RANS. It numerically resolves the large-scale vortices while using sub-grid stress models to account for the effects of unresolved small-scale vortices by resolved larger scales, resulting in lower computational expenses than DNS but higher accuracy than RANS. In LES, the Smagorinsky model [9], Dynamic Smagorinsky model [10] and WALE model [11] are widely employed. The Smagorinsky model is especially favored for its simplicity. However, despite its simplicity and established reputation, the model has at least one significant drawback: it tends to overestimate eddy viscosity in the presence of strong background shear, resulting in a non-zero eddy viscosity at the wall. The Smagorinsky model is defined as follows:

$$v_t = C_s \Delta^2 \bar{\mathrm{S}} = C_s \Delta^2 \sqrt{2 \bar{S}_{ij} \bar{S}_{ij}} \tag{2}$$

where, v_t is the eddy viscosity, C_s is a model coefficient, Δ is a characteristic length scale often determined by the filtering width of the mesh, and $\bar{S}_{ij} = \frac{1}{2}\left(\frac{\partial \bar{u}_i}{\partial x_j} + \frac{\partial \bar{u}_j}{\partial x_i}\right)$ represents the filtered rate-of-strain tensor.

Since the eddy viscosity is caused by vortex and Liutex correctly represents vortex, Wang [12] introduced a Liutex-based sub-grid stress model, utilizing a G3 method. The model is defined as follows:

$$v_t = C_v \Delta^2 \bar{\mathrm{R}} \tag{3}$$

where, C_v is a coefficient, Δ is the filtering length scale and $\bar{\mathrm{R}}$ is Liutex magnitude, which is defined as,

$$\bar{\mathrm{R}} = \sqrt{\bar{\mathrm{R}}_1^2 + \bar{\mathrm{R}}_2^2 + \bar{\mathrm{R}}_3^2} \tag{4}$$

where $\bar{R}_1$, $\bar{R}_2$ and $\bar{R}_3$ are filtered Liutex components.

The purpose of this study is to apply the new Liutex-based sub-grid model in the backward facing step flow, the channel flow and flat plate boundary transition, compared with Smagorinsky model and LES with no model. It is also proved in this paper theoretically that Liutex is zero at the no-slip boundary so that the Liutex-based eddy viscosity is consistent with physics.

II. Case Set Up

A. Backward Step Flow

The turbulent flow over a backward step at Reynolds number $Re_h = 5000$ is set up and the computational domain consists of streamwise length $L_x = 20h$, spanwise length $L_y = 4h$ and normal length $L_z = 11h$, where h is the step height. The coordinate system is oriented in the way that the x-axis represents the streamwise direction, the y-axis indicates the spanwise direction, and the z-axis corresponds to the wall-normal direction. 20,000 recorded data sets of turbulent flow obtained from DNS of a flat plate boundary transition [13] are imposed into to the inlet flow. In the spanwise direction, the periodic conditions are applied. Non-slipping conditions are imposed on both the wall at the bottom and the step. The LES grid dimensions are 960×64×120, corresponding to the number of grid points in the streamwise, spanwise, and wall-normal directions. Additionally, grids are locally refined in the wall-normal and

Downloaded by Emran Hossen on March 25, 2025 | http://arc.aiaa.org | DOI: 10.2514/6.2025-0073

streamwise direction, while the spanwise dimensions remain uniform. Fig. 1 exhibits the computational domain and Fig. 2 shows the illustration of grids refinement near the step corner and bottom wall.

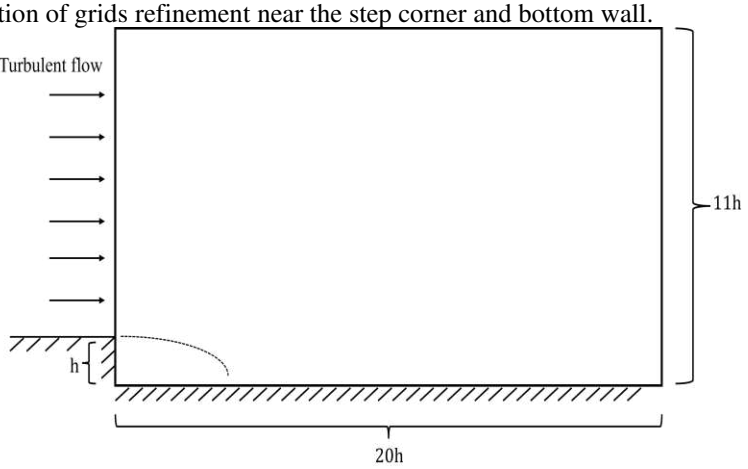

Fig. 1 Computation domain of backward step flow

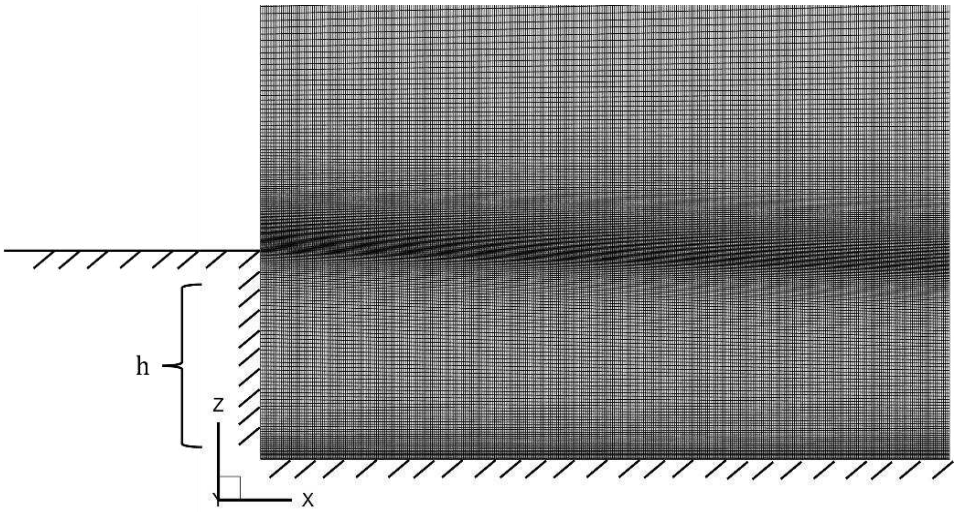

Fig. 2 Grids refinement near the step corner and bottom wall

At the streamwise and normal wall direction, a sixth-order compact scheme is used for spatial discretization. The sixth-order compact scheme is given as follows:

$$\frac{1}{3}f'_{i-1} + f'_{i-1} + \frac{1}{3}f'_{i-1} = \frac{1}{h}\left(-\frac{1}{36}f_{i-2} - \frac{7}{9}f_{i-1} + \frac{7}{9}f_{i+1} + \frac{1}{36}f_{i+2}\right) \tag{5}$$

Where $i = 3, \ldots, N-2$ for the internal points, f'_i is the derivative at point i. The fourth-order compact scheme is used at points $i = 2$ and $N-1$, and the third-order one-sided compact scheme is used at the boundary. An implicit sixth-order compact scheme for space filtering is applied to the primitive variables after a specified number of time steps. For time advancement, a third-order TVD Runge–Kutta scheme is applied as follows:

$$\boldsymbol{Q}^{(0)} = \boldsymbol{Q}^{n} \tag{6}$$

$$\boldsymbol{Q}^{(1)} = \boldsymbol{Q}^{(0)} + \Delta t \boldsymbol{R}^{(0)} \tag{7}$$

$$\boldsymbol{Q}^{(2)} = \frac{3}{4}\boldsymbol{Q}^{(0)} + \frac{1}{4}\boldsymbol{Q}^{(1)} + \frac{2}{4}\Delta t \boldsymbol{R}^{(1)} \tag{8}$$

$$\boldsymbol{Q}^{(3)} = \frac{1}{3}\boldsymbol{Q}^{(0)} + \frac{2}{3}\boldsymbol{Q}^{(2)} + \frac{1}{3}\Delta t \boldsymbol{R}^{(2)} \tag{9}$$

$$\boldsymbol{Q}^{n+1} = \boldsymbol{Q}^{(3)} \tag{10}$$

B. Channel Flow

Downloaded by Emran Hossen on March 25, 2025 | http://arc.aiaa.org | DOI: 10.2514/6.2025-0073

Fig. 3 shows the computational domain and grids of the channel flow. The lengths of the computational domain are 4m, 2m and 2m in the x, y, z directions respectively. This case is a statistically-developing internal flow through parallel walls. The Reynolds number based on the friction velocity is 395. The characteristic length (channel half-height) is $\delta = 1.0$ m and the bulk velocity is $U_b = 0.1335\, m/s$. The kinematic viscosity of the fluid is $\nu = 2.0 \times 10^{-5}\, m^2/s$. The grids include 80×70×60 points in the x, y, and z directions, respectively. The grids are uniformly distributed in the x and z directions, while it is refined near the walls in the y direction. The Δ_y^+, Δ_x^+, and Δ_z^+ values of the first grid layer are 1.1, 49.6, and 15.1, respectively. No-slip boundary conditions are applied on the upper and lower walls (in the y-direction), while periodic boundary conditions are applied in the other two directions. The pressure term is adjusted during the numerical simulations to keep the flow rate constant.

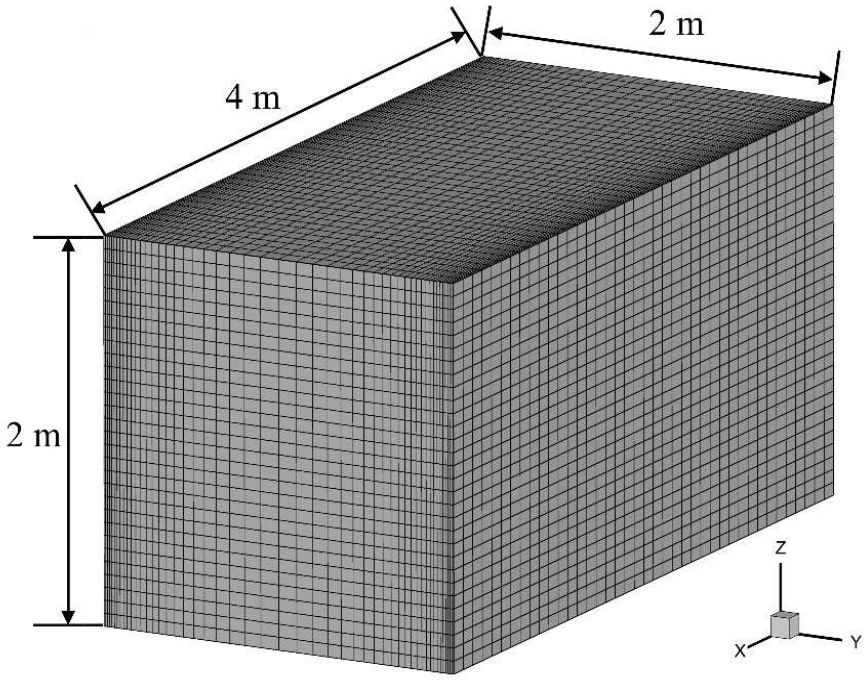

Fig. 3 Computational domain and grids of the channel flow

Downloaded by Emran Hossen on March 25, 2025 | http://arc.aiaa.org | DOI: 10.2514/6.2025-0073

C. Flat Plate Boundary Transition

Fig. 4 shows the physical domain of the simulation. In Fig. 4, x_{in} refers to the distance between the inlet of the domain and the leading edge. L_x and L_y represent the streamwise and spanwise lengths of the domain respectively. L_{zin} denotes the height of the inlet. $1920 \times 128 \times 241$ grids are used for DNS simulation while $960 \times 32 \times 61$ grids are used for LES simulations. The parameters of the simulations are as follows. $x_{in} = 300.79\delta_{in}$, $L_x = 798.03\delta_{in}$, $L_y = 22\delta_{in}$, where δ_{in} is the displacement boundary thickness of inflow. $Ma_\infty = 0.5$, $Re = 1000$, $T_w = 273.15K$ and $T_\infty = 273.15K$, where Ma_∞ represents Mach number, Re represents Reynolds number, T_w represents wall temperature and T_∞ represents free stream temperature. The same numerical methods described in the backward step flow are used in this case. The inflow is the Blasius solution plus Tollmien-Schlichting waves.

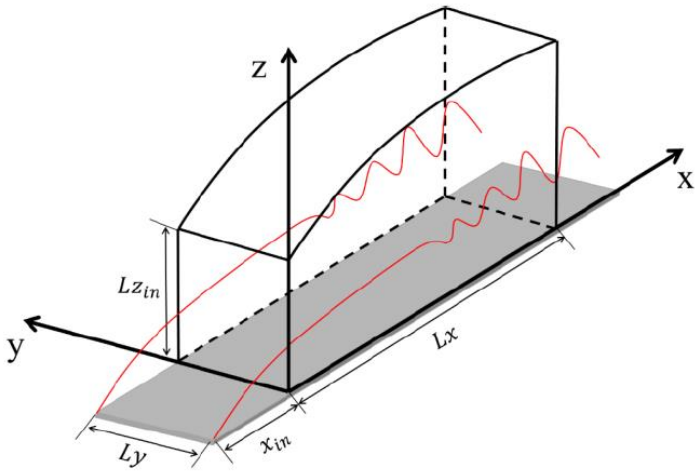

Fig. 4 Physical domain of simulation

III. Results and Discussions

A. Result of channel flow and proof of Liutex being zero at no-slip boundary

Without losing generality, we assume that x-y plane is the no-slip boundary and z is the direction normal to the boundary plane. Because of the no-slip boundary condition, for a point at the wall surface,

$$\frac{\partial u}{\partial x} = \frac{\partial u}{\partial y} = \frac{\partial v}{\partial x} = \frac{\partial v}{\partial y} = \frac{\partial w}{\partial x} = \frac{\partial w}{\partial y} = 0 \tag{11}$$

Thus, its velocity gradient tensor is:

$$\begin{bmatrix} 0 & 0 & \frac{\partial u}{\partial z} \\ 0 & 0 & \frac{\partial v}{\partial z} \\ 0 & 0 & \frac{\partial w}{\partial z} \end{bmatrix} \tag{12}$$

Apparently, Eq. 12 has three real eigenvalues leading to a zero Liutex. As a result, Liutex-based sub-grid stress must be zero. Based on the same velocity gradient tensor Eq. 12, the eddy viscosity estimated by Smagorinsky model is

$$v_t = C_s \Delta^2 \bar{S} = C_s \Delta^2 \sqrt{\left(\frac{\partial u}{\partial z}\right)^2 + \left(\frac{\partial v}{\partial z}\right)^2 + 2\left(\frac{\partial w}{\partial z}\right)^2} \tag{13}$$

which is not guaranteed to be zero.

The results of our simulation are consistent with theoretical analysis. Fig. 5 and Fig. 6 present the eddy viscosity distributions of Smagorinsky and Liutex-based sub-grid model for the channel flow respectively. One can clearly see that for Smagorinsky sub-grid model, eddy viscosity is large near the wall surface (the left and right sides) which is inconsistent with physics. On the contrary, for Liutex-based sub-grid model, eddy viscosity is zero near the wall surfaces (the left and right sides), which is consistent with the physics. A clearer comparison can be seen in Fig. 7 which depicts the relation between eddy viscosity and y/h. The eddy viscosity of Smargorinsky sub-grid model is quite large near the wall while that of Liutex-base mode is zero.

Downloaded by Emran Hossen on March 25, 2025 | http://arc.aiaa.org | DOI: 10.2514/6.2025-0073

Downloaded by Emran Hossen on March 25, 2025 | http://arc.aiaa.org | DOI: 10.2514/6.2025-0073

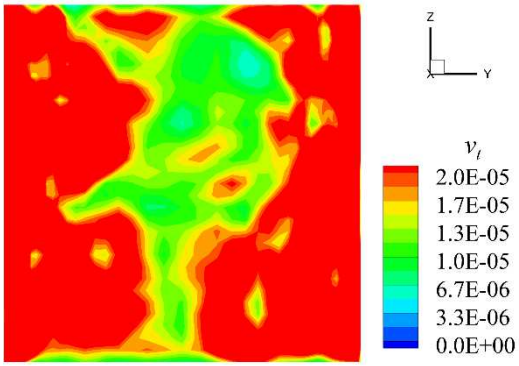

Fig. 5 Eddy viscosity distribution of Smagorinsky sub-grid model for the channel flow.

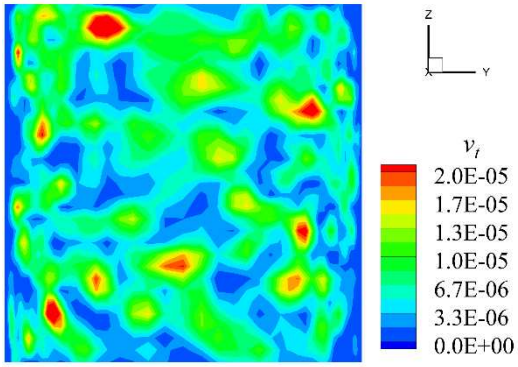

Fig. 6 Eddy viscosity distribution of Liutex-based sub-grid model for the channel flow.

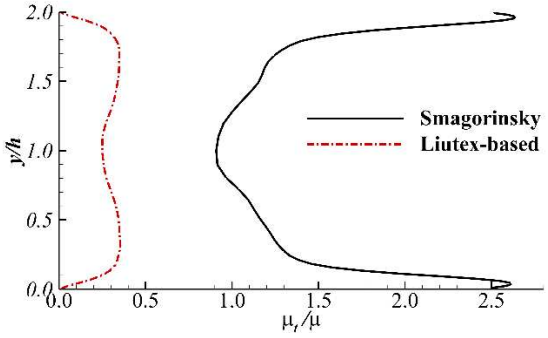

Fig. 7 Eddy viscosity distributions of different sub-grid models for the channel flow.

Fig. 8 shows time- and spanwise-averaged streamwise velocity profiles in wall coordinates, clearly showing that Liutex-based model fits log law better than Smagorinsky model.

Downloaded by Emran Hossen on March 25, 2025 | http://arc.aiaa.org | DOI: 10.2514/6.2025-0073

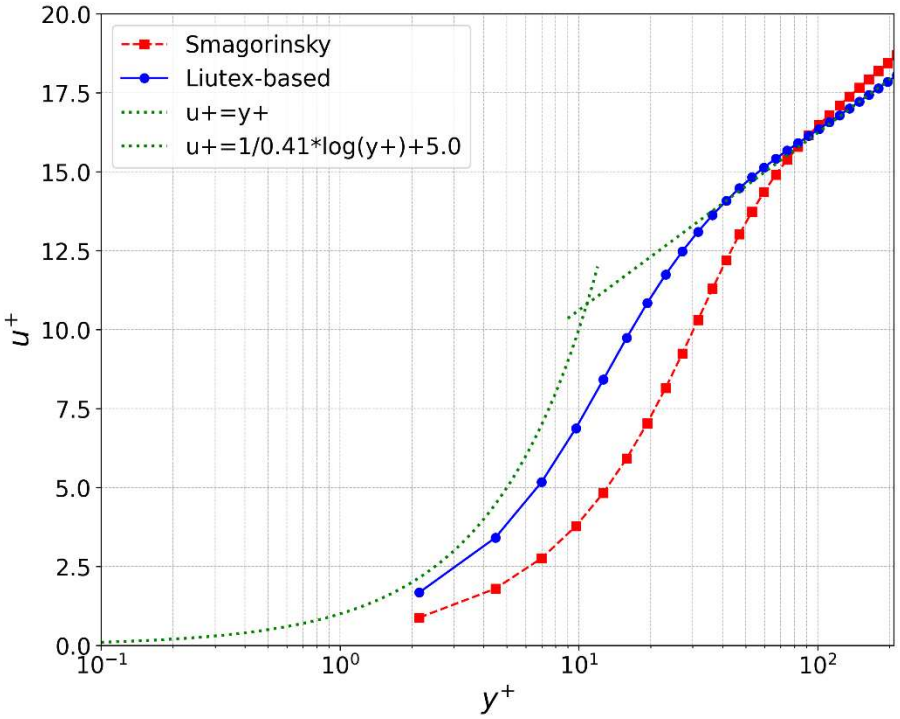

Fig. 8 Time- and spanwise-averaged streamwise velocity profiles in wall coordinates for the channel flow

B. Result of the Backward Step Flow

The reattachment lengths of Smagorinsky model, Liutex-based model and using no model are 5.98h, 6.27h and 5.8h. Le's[14] DNS at a close Renolds number shows the reattachment length is 6.28h. Liutex-based model is the closet to Le's DNS result. Fig. 9 shows the near-wall time- and spanwise-averaged velocity profiles plotted in semi-logarithmic coordinates at x=18h. $u^+ = y^+$ and $u^+ = \frac{1}{0.41}\ln(y^+) + 5$ are also plotted for the comparison of log-law. After applying LES models, the curves are closer to the log law than using no model. Liutex-based model matches the log law better than Smagorinsky model and using no model.

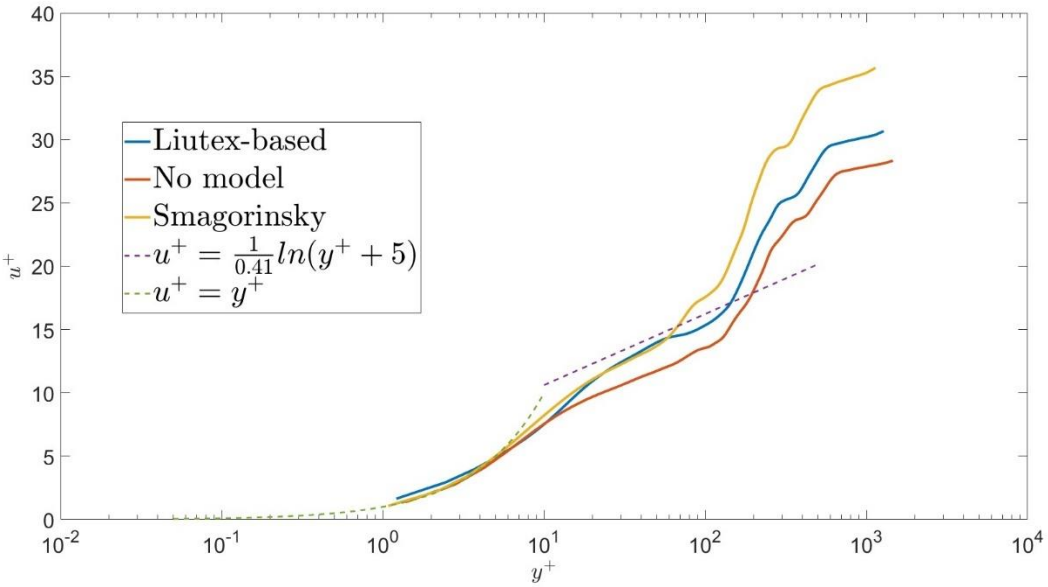

Fig. 9 Time- and spanwise-averaged streamwise velocity profiles in wall coordinates at $x = 19h$.

Fig.10 to Fig. 12 exhibit the time- and spanwise-averaged streamlines of Smagorinsky model, Liutex-based model and using no model. The zoomed-in figures near the step corners are also provided. The secondary vortex can be seen in all of them. However, a third vortex can only be observed for Liutex-based model which shows Liutex-based model has higher resolution.

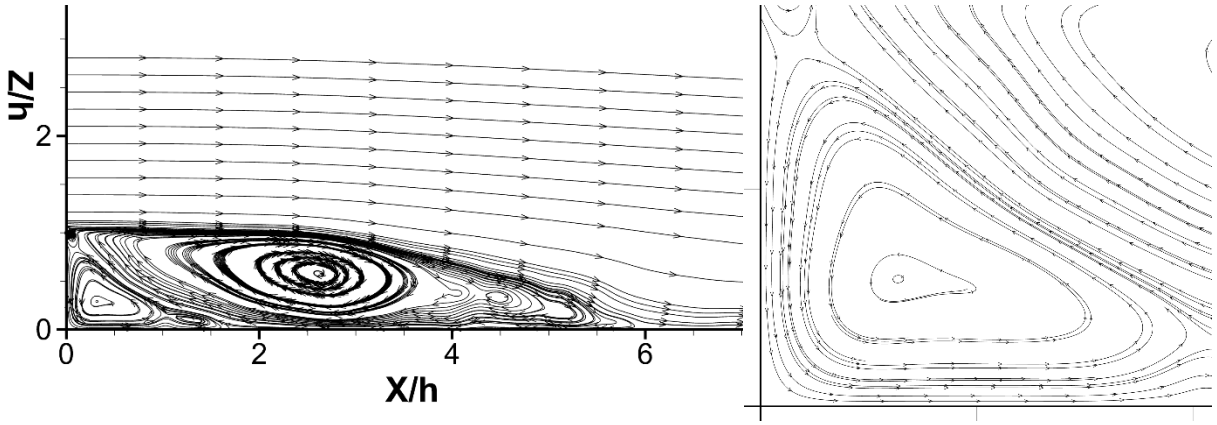

(a) (b)

Fig. 10 Time- and spanwise- averaged streamlines of Smagorinsky model. (a) general. (b) near the step corner.

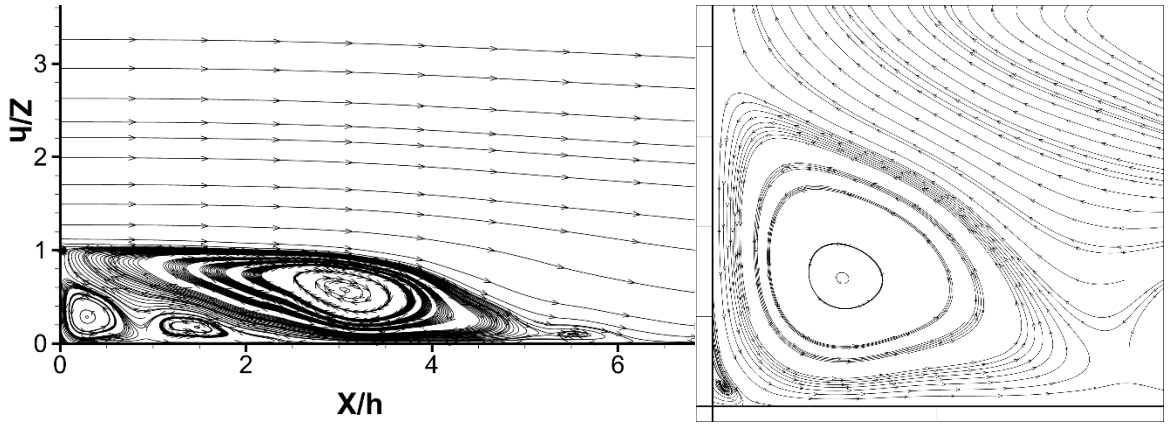

(a) (b)

Fig. 11 Time- and spanwise- averaged streamlines of Liutex-based model. (a) general. (b) near the step corner.

Downloaded by Emran Hossen on March 25, 2025 | http://arc.aiaa.org | DOI: 10.2514/6.2025-0073

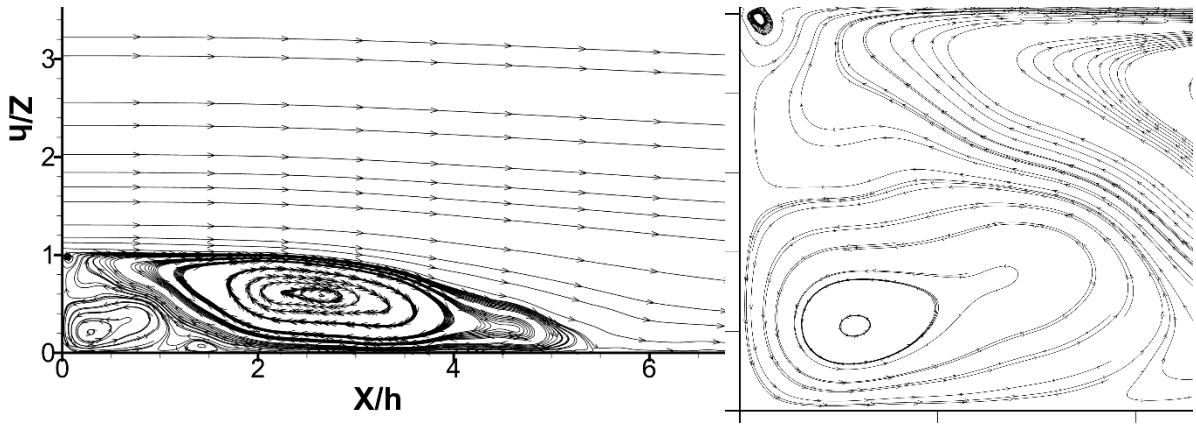

(a) (b)

Fig. 12 Time- and spanwise- averaged streamlines of using no model. (a) general. (b) near the step corner.

Downloaded by Emran Hossen on March 25, 2025 | http://arc.aiaa.org | DOI: 10.2514/6.2025-0073

C. Result of Flat Plate Boundary Later Transition

Fig. 13 to Fig. 15 show the time- and spanwise-averaged velocity profiles near the wall as well as $u^+ = 2.75\ln(y^+) + 5.2$, plotted in semi-logarithmic coordinates, at x=700, x=800 and x=900. For all locations, Liutex-based model is the best one that matches the DNS result, while no model case is the worst and Smagorinsky model is better than no model. The DNS and Liutex-based model results fit the log-law very well while Smagorinksy model and no model overestimate u^+.

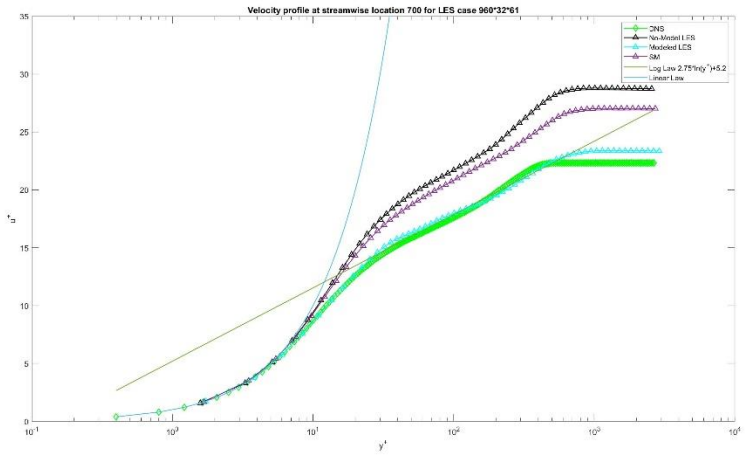

Fig. 13 Time- and spanwise-averaged velocity profiles at x=700

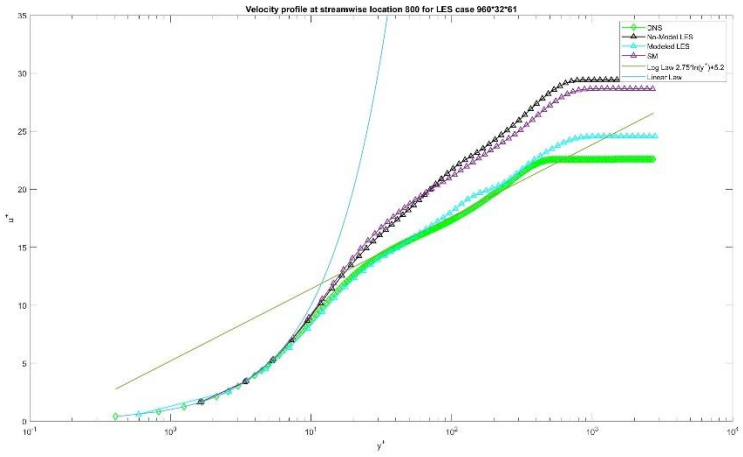

Fig. 14 Time- and spanwise-averaged velocity profiles at x=800

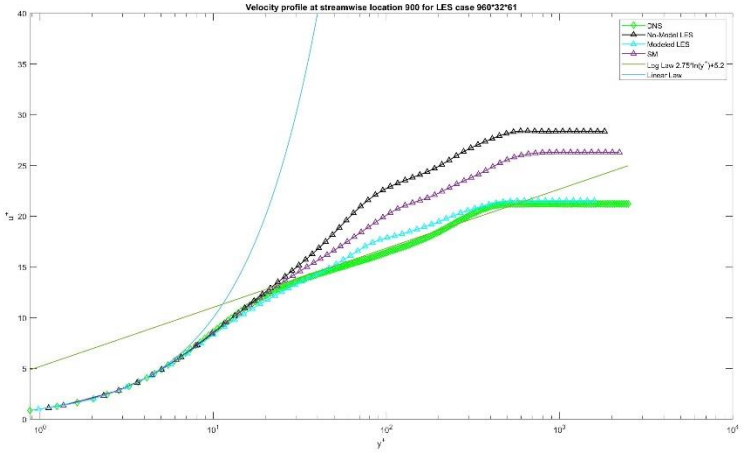

Fig. 15 Time- and spanwise-averaged velocity profiles at x=900

IV. Summary

This paper applies Liutex-based LES model to turbulent flow over a backward step, the channel flow and flat plate boundary layer transition. The simulation results show that Liutex-based SGS model more accurately estimates the eddy viscosity at the wall boundary. The theoretical analysis also provides that the eddy viscosity estimated by Liutex-based model is zero near the wall surface while that estimated by Smagorinsky is large which is inconsistent with physics. Any model which estimates non-zero eddy viscosity in the laminar sublayer near the wall surface is inconsistent with physics. The streamlines, velocity profiles and reattachment lengths for the simulations of backward step flow are also reported. Only Liutex-based model can resolve a third vortex near the step corner and the reattachment length of Liutex-based model is the closest to Le's DNS result. The result of flat plate boundary transition shows that Liutex-based model is the one closest to DNS and only uses $\frac{1}{32}$ grids as DNS. In summary, the new Liutex-based model is intrinsic consistent with physics and achieves good results in simulations.

Acknowledgments

The authors appreciate the support from the National Science Foundation. This study is supported by NSF # 2422573. The authors are grateful to Texas Advanced Computation Center (TACC) for providing computing resources.

Downloaded by Emran Hossen on March 25, 2025 | http://arc.aiaa.org | DOI: 10.2514/6.2025-0073

References

[1] Liu, C., Gao, Y., Tian, S., and Dong, X., "Rortex—A New Vortex Vector Definition and Vorticity Tensor and Vector Decompositions," *Physics of Fluids*, Vol. 30, No. 3, 2018, p. 035103. https://doi.org/10.1063/1.5023001

[2] Liu, C., Gao, Y., Dong, X., Wang, Y., Liu, J., Zhang, Y., Cai, X., and Gui, N., "Third Generation of Vortex Identification Methods: Omega and Liutex/Rortex Based Systems," *Journal of Hydrodynamics*, Vol. 31, No. 2, 2019, pp. 205–223. https://doi.org/10.1007/s42241-019-0022-4

[3] Shrestha, P., Nottage, C., Yu, Y., Alvarez, O., and Liu, C., "Stretching and Shearing Contamination Analysis for Liutex and Other Vortex Identification Methods," *Advances in Aerodynamics*, Vol. 3, No. 1, 2021, p. 8. https://doi.org/10.1186/s42774-020-00060-9

[4] Kolář, V., and Šístek, J., "Stretching Response of Rortex and Other Vortex-Identification Schemes," *AIP Advances*, Vol. 9, No. 10, 2019, p. 105025. https://doi.org/10.1063/1.5127178

[5] Gao, Y., and Liu, C., "Rortex Based Velocity Gradient Tensor Decomposition," *Physics of Fluids*, 2019.

[6] Wang, Y., Gao, Y., Liu, J., and Liu, C., "Explicit Formula for the Liutex Vector and Physical Meaning of Vorticity Based on the Liutex-Shear Decomposition," *Journal of Hydrodynamics*, Vol. 31, No. 3, 2019, pp. 464–474. https://doi.org/10.1007/s42241-019-0032-2

[7] Temam, R., "Navier-Stokes Equations: Theory and Numerical Analysis," American Mathematical Society, 2024.

[8] Stokes, G. G., "On the Effect of the Internal Friction of Fluids on the Motion of Pendulums," 1851.

[9] Smagorinsky, J., "GENERAL CIRCULATION EXPERIMENTS WITH THE PRIMITIVE EQUATIONS: I. THE BASIC EXPERIMENT*," *Monthly Weather Review*, Vol. 91, No. 3, 1963, pp. 99–164. https://doi.org/10.1175/1520-0493(1963)091<0099:GCEWTP>2.3.CO;2

[10] Germano, M., Piomelli, U., Moin, P., and Cabot, W. H., "A Dynamic Subgrid-Scale Eddy Viscosity Model," *Physics of Fluids A: Fluid Dynamics*, Vol. 3, No. 7, 1991, pp. 1760–1765. https://doi.org/10.1063/1.857955

[11] Nicoud, F., and Ducros, F., "Subgrid-Scale Stress Modelling Based on the Square of the Velocity Gradient Tensor," *Flow, Turbulence and Combustion*, Vol. 62, 1999, pp. 183–200.

[12] Ding, Y., Pang, B., Yan, B., Wang, Y., Chen, Y., and Qian, Y., "A Liutex-Based Subgrid Stress Model for Large-Eddy Simulation," *Journal of Hydrodynamics*, Vol. 34, No. 6, 2022, pp. 1145–1150. https://doi.org/10.1007/s42241-023-0085-0

[13] Wang, Y., Yang, Y., Yang, G., and Liu, C., "DNS Study on Vortex and Vorticity in Late Boundary Layer Transition," *Communications in Computational Physics*, Vol. 22, No. 2, 2017, pp. 441–459. https://doi.org/10.4208/cicp.OA-2016-0183

[14] Le, H., Moin, P., and Kim, J., "Direct Numerical Simulation of Turbulent Flow over a Backward-Facing Step," *Journal of Fluid Mechanics*, Vol. 330, 1997, pp. 349–374. https://doi.org/10.1017/S0022112096003941

Downloaded by Emran Hossen on March 25, 2025 | http://arc.aiaa.org | DOI: 10.2514/6.2025-0073